JOURNAL OF GEOPHYSICAL RESEARCH, VOL. 114, A02205, doi:10.1029/2008JA013100, 2009

Regulation of the centrifugal interchange cycle in Saturn's inner magnetosphere

A. Kidder,[1] R. M. Winglee,[1] and E. M. Harnett[1]

Received 16 February 2008; revised 16 August 2008; accepted 16 October 2008; published 7 February 2009.

[1] Multifluid modeling of Saturn's magnetosphere produces the first numerical simulation showing the development of hot, tenuous plasma from the plasma sheet interchanging with cold, denser plasma from the inner magnetosphere. Individual injection events are seen regularly by Cassini, but with a single observation it is impossible to determine the global distribution. Multifluid simulations enable us to characterize the growth and development of not merely one injection event but show that it is a global process dependent on both the plasma distribution of ions from Enceladus and forcing by solar wind conditions. Development of the interchange arises in a fashion similar to a Rayleigh-Taylor instability, except that the heavy ions are being driven outward not by gravity but by centrifugal forces. Interplanetary magnetic field (IMF) parallel to the planetary magnetic field reduces centrifugal forcing, whereas antiparallel IMF increases the forcing, by altering the bowl-like shape of the plasma sheet. However, the interchange instability also develops under normally quiet parallel IMF conditions when the mass loading of the Enceladus torus is increased. The total number of interchange events is 1–2 higher for the antiparallel case versus the increased mass case. Interchange develops in the vicinity of 7 R_S, and once the fingers of cold plasma reach $\sim$12–14 R_S (close to the inner edge of the plasma sheet) they spread in the azimuthal direction, because of the fact that the magnetic field is too weak to keep the fingers solidly locked in rotation. The derived energy characteristics of the interchanging plasma are shown to be consistent with Cassini data.

Citation: Kidder, A., R. M. Winglee, and E. M. Harnett (2009), Regulation of the centrifugal interchange cycle in Saturn's inner magnetosphere, *J. Geophys. Res.*, *114*, A02205, doi:10.1029/2008JA013100.

1. Introduction

[2] During its first two orbits of Saturn, the Cassini spacecraft observed plasma and magnetic signatures near the equatorial plane consistent with the inward movement of hot, tenuous plasma [*Burch et al.*, 2005; *Mauk et al.*, 2005; *André et al.*, 2005; *Persoon et al.*, 2005]. Within these injection regions, CAPS instruments observed the temperature of the electron and ion populations to increase by an order of magnitude and the densities of each decrease by a factor of two. The magnetic field magnitude also increased by $\sim$3 nT with respect to the background magnetic field [*Burch et al.*, 2007]. These temperature, density, magnetic field and energy signatures are believed to be characteristic of the inward movement of hot interchanging plasma in Saturn's inner magnetosphere; although some plasma injections from Rev A [*André et al.*, 2007] exhibit decreased magnetic pressure, and were theorized to be a result of their higher latitudes up out of the equatorial plane. Injection events have been observed at all local times at Saturn, and do not appear to exhibit any preference for a particular sector [*Hill et al.*, 2005]. It has been suggested that large-scale, broad outward flows of cool dense plasma are responsible for conserving the flux of this injected plasma [*Sittler et al.*, 2006], but are much less frequently observed than their injection counterparts. Recently observed butterfly-shaped pitch angle distributions have been put forth as evidence of this flux-balancing outward flow [*Burch et al.*, 2007].

[3] Interchanging flux tubes have been detected at Jupiter [*Kivelson et al.*, 1997], another example of an inner magnetosphere strongly controlled by rotation. Both Saturn and Jupiter have inner magnetospheres which include an ionized torus of plasma (from Io at Jupiter and Enceladus at Saturn) that is continually being replenished. For Jupiter, Galileo data shows the plasma in the Io torus can interchange [*Krupp et al.*, 2004], as the spacecraft detected events near Io where regions of less dense plasma with a stronger magnetic field appeared to be injected toward Jupiter [*Mauk et al.*, 1997; *Kivelson et al.*, 1997]. Examining the differences in how and when injection events occur at these two planets will help distinguish the physical processes that regulate centrifugal interchange.

[4] Global MHD simulations have been used to investigate the overall shape of Saturn's magnetosphere, including the position of the bow shock and magnetopause as a function of the solar wind conditions [*Hansen et al.*,

[1]Department of Earth and Space Sciences, University of Washington, Seattle, Washington, USA.

0148-0227/09/2008JA013100$09.00

2000, 2005]. Another MHD study has looked at the formation of vortices during many different IMF conditions [*Fukazawa et al.*, 2007]. These studies demonstrated the importance of the IMF in determining the flows and magnetic fields within the magnetosphere.

[5] Multifluid modeling enables us to study how different sources of light and heavy ion populations affect this broad outwelling of cool plasma and narrow injection of hotter plasma, while still retaining a model large enough to encompass the whole Saturnian magnetosphere. In this paper we focus on the inner magnetosphere (out to $\sim$18 R_S, with 1 R_S = 62,268 km) in order to quantify how the centrifugal interchange cycle begins and evolves and compare it with the observed features described above. It is necessary to resolve the entire magnetosphere in three dimensions, from the bow shock to $\sim$60 R_S downtail, to examine the extent to which the IMF can perturb what appears to be a rotationally dominated magnetosphere.

[6] In this paper we use a multifluid model to quantify how interchanging magnetospheric plasma is affected indirectly by the orientation of the IMF, or the concentration an of inner magnetospheric Enceladus source of heavy ions. The work is focused on the development and growth of the interchange instability over multiple rotations of the planet and it is shown that heavy and light ion dynamics lead to quantitatively different pictures of the inner magnetosphere than that which is predicted by a single-fluid treatment provided by MHD. We are able to match bulk characteristics of the injection events by comparing the energy and fluxes in our model spectrograms with Cassini-observed ion and electron spectrograms. We describe the extent to which the orientation of the IMF influences the development of the interchange instability. We next examine how increasing the concentration of heavy ions in the vicinity of Enceladus increases the total number of interchanging flux tubes over both the parallel IMF and antiparallel IMF cases. Mass loading of the Kronian magnetosphere by the Enceladus ion torus and forcing from the solar wind control the point at which the Kronian plasma deviates from a rotationally driven to an externally driven system. In other words, both the inner boundary conditions and the solar wind forcing play important roles in the development of the interchange instability.

2. Model

[7] If the effect of the solar wind and IMF conditions on centrifugal interchange events is to be examined it is necessary to model plasma flow on a global scale while still incorporating the dynamics of different mass ions. In order to determine which variables regulate the interchange cycle, we look past MHD, which is a single-fluid model, and include multiple ion populations with individual temperatures and velocities for each species. The multifluid treatment is a global model using three ion fluids and an electron fluid; the model employed here has been used in terrestrial applications, e.g., to show the importance of O^+ outflow during storms [*Winglee*, 2004], as well as to study outer planet satellites, including ion energy distributions at Ganymede [*Paty and Winglee*, 2006], asymmetric pickup and mass loading of ions at Titan [*Snowden et al.*, 2007], and the incorporation of charge exchange in both ion and neutral fluids around Enceladus [*Paty et al.*, 2007]. The inclusion of mass effects in the model by using ion cyclotron effects in the full conservation of momentum equation and a generalized Ohm's law makes it possible to track differential heating and acceleration of different ions.

2.1. Multifluid Equations

[8] The multifluid equations (1)–(3) track the different ion species as individual fluids through separate equations for mass, momentum and pressure. The subscript α denotes an individual ion or electron population.

$$\frac{\partial \rho_\alpha}{\partial t} + \nabla \cdot (\rho_\alpha \vec{\mathrm{v}}_\alpha) = 0 \tag{1}$$

$$\rho_\alpha \frac{d\vec{\mathrm{v}}_\alpha}{dt} = q_\alpha n_\alpha \left(\vec{\mathrm{E}} + \vec{\mathrm{v}}_\alpha \times \vec{\mathrm{B}}\right) - \nabla \mathrm{P}_\alpha - \left(\frac{GM_S}{R_S^2}\right)\rho_\alpha \vec{r} \tag{2}$$

$$\frac{\partial \mathrm{P}_\alpha}{\partial t} = -\gamma \nabla \cdot (\mathrm{P}_\alpha \vec{\mathrm{v}}_\alpha) + (\gamma - 1)\vec{\mathrm{v}}_\alpha \cdot \nabla \mathrm{P}_\alpha \tag{3}$$

where ρ_α is the mass density, $\vec{\mathrm{v}}_\alpha$ the bulk velocity, n_α the number density and q_α the charge. G is the gravitational constant, M_S the mass of Saturn, $\vec{E}$ the electric field, $\vec{B}$ the magnetic field. P_α is the pressure for each ion species and γ is the ratio of specific heats (5/3).

[9] The electron dynamics are described with a pressure equation where the electron velocity is assumed to be determined by drift motion (i.e., $dv_e/dt = 0$) in (2).

$$\frac{\partial \mathrm{P}_e}{\partial t} = -\gamma \nabla \cdot (\mathrm{P}_e \vec{\mathrm{v}}_{de}) + (\gamma - 1)\vec{\mathrm{v}}_{de} \cdot \nabla \mathrm{P}_e \tag{4}$$

[10] Approaching this limit the modified Ohm's law becomes:

$$\vec{\mathrm{E}} = -\sum_i \frac{n_i}{n_e}\vec{\mathrm{v}}_i \times \vec{\mathrm{B}} + \frac{\vec{\mathrm{J}} \times \vec{\mathrm{B}}}{en_e} - \frac{\nabla \mathrm{P}_e}{en_e} + \eta(\vec{r})\vec{\mathrm{J}} \tag{5}$$

where n_e is the electron number density, e the electron charge, $\vec{J}$ the current density and η the resistivity, added to allow finite conductivity only in the ionosphere.

[11] Everywhere else this number is zero, so there is no anomalous resistivity in our model. Modeling the ion and electron components separately allows us to retain the Hall and pressure gradient terms in Ohm's law (5), which are sufficient to drive reconnection. On substituting (5) into the momentum equation we obtain:

$$\rho_\alpha \frac{d\vec{\mathrm{v}}_\alpha}{dt} = \frac{q_\alpha n_\alpha}{en_e}\left(\vec{\mathrm{J}} \times \vec{\mathrm{B}} - \nabla \mathrm{P}_e\right) - \nabla \mathrm{P}_\alpha + q_\alpha n_\alpha \left(\vec{\mathrm{v}}_\alpha - \sum_i \frac{n_i}{n_e}\vec{\mathrm{v}}_i\right) \times \vec{\mathrm{B}} + q_\alpha n_\alpha \eta \vec{\mathrm{J}} - \left(\frac{GM_S}{R_S^2}\right)\rho_\alpha \vec{r} \tag{6}$$

If one assumes a single ion species or a single velocity for all the species, then (5) reduces to the ideal MHD equation. For different ion species with different velocities, however,

the middle term in (6), neglected in MHD, is in fact nonzero and will contribute to the development of ion cyclotron effects.

2.2. Boundary Conditions

[12] The equations for the multifluid treatment are solved using a second-order Runge-Kutta method [*Butcher*, 1987], on a nested grid. The nested grid consists of five boxes centered around the planet, with the inner boundary at 2.25 R_S. The coordinate system is such that x is in Saturn's equatorial plane and a positive value points away from the Sun. The positive z direction points along the magnetic north pole, and the y coordinate completes the system. The z direction is also aligned with Saturn's rotation axis. The inner magnetosphere (from ±15 R_S in the x and y directions and ±7.5 R_S in the z direction) is resolved to 1/4 R_S and the outer magnetosphere is covered over a range of 480 R_S, 76 R_S sunward and 404 R_S downtail in the x direction, ±240 in the y direction and ±120 in the z direction.

2.3. Initial Conditions

[13] In the simulation, the solar wind is blown in from the negative x direction with a velocity of ~400 km/s and is angled 28° upward, to account for Saturn's tilt relative to its orbital plane. The solar wind has been assigned a density of 0.05 protons cm^{-3}, a temperature of 1.4 eV and an IMF of magnitude ±0.3 nT in $\hat{z}$. The model is first run for 30 h at zero IMF to establish an appropriate equilibrium for the magnetosphere. IMF is then propagated in for 18 more hours before the times for the results shown in this paper.

[14] The three ion components are H^+, assumed to be from the solar wind or Saturn's ionosphere, a medium ion such as C^+, N^+ or O^+ of mass 16 amu, (hereafter referred to as CNO^+), and a 32 amu heavy species such as N_2^+ or O_2^+ (hereafter referred to as Hvy^+). The Enceladus ion source is incorporated in the model by placing an ion torus of CNO^+ with a density of 2 cm^{-3} at Enceladus' orbit, consistent with observations [*Young et al.*, 2005]. The plasma torus is initialized on field lines that enclose Enceladus' L shell at 4 ± 0.5. This yields an extended torus that would be associated with ionization of neutrals well away from Enceladus. Heavy ions are initialized in this region as a tracer ion species with a density of 0.25 cm^{-3} [*Young et al.*, 2005]. A predominantly H^+ ionosphere is assumed at the inner boundary of 2.25 R_S, representing Saturn's ionosphere. This density is held constant at a value of 50 cm^{-3}. All ion fluids have a Maxwellian distribution. The heavy ion species is also used to examine the interaction of the Kronian plasma with Titan as described by R. M. Winglee et al. (Modification of Titan's ion tail and the Kronian magnetosphere: Coupled magnetospheric simulations, submitted to *Journal of Geophysical Research*, 2008). The ionospheric temperature gradient ranges from 18 eV at the equator to 1 eV at the poles. The temperature is also held constant at the inner boundary. Each species evolves with different temperatures and velocities away from the inner boundary as determined by the formulas in the previous section. The inner boundary assumes a plasma with prescribed density and temperature but no bulk velocity, which leads to a small thermal, or polar, wind. Enhanced outflow is produced as a result of the convection of magnetic field through the system. Saturn is assumed to have a dipolar magnetic field with the opposite polarity of Earth, and an equatorial field strength equal to 21,000 nT at the inner boundary.

[15] We examine two configurations of the IMF with the Enceladus density described above: antiparallel and parallel IMF at ±0.3 nT. IMF parallel to the planetary field leads to a thicker plasma sheet, reduced magnetospheric convection and a corresponding reduction/cessation of the development of interchange fingers, as the Kronian plasma is more bowl shaped at 20–40 R_S. The antiparallel IMF configuration exhibits very strong finger growth, and because of thinning of the current sheet, the bowl-shaped plasma sheet has a less steep angle than in the parallel case. Next, we consider an Enceladus ion torus in which elevated densities (double the concentration of both CNO^+ and Hvy^+) are assumed, which may occur for example during active plume ejection from Enceladus. This increased density shows that the torus mass is another factor in controlling the development of the interchange fingers.

3. Results

3.1. Interchange Fingers Develop Through Rayleigh-Taylor Instability

[16] Finger-like extensions of cool plasma do not readily appear in the equatorial plane of the inner magnetosphere under conditions of parallel IMF, but are seen to develop during IMF that is antiparallel to Saturn's planetary magnetic field. This interchange of dense inner plasma with tenuous plasma is a Rayleigh-Taylor (RT) type instability, in that a heavy plasma (Enceladus ion torus, CNO^+) is on top of lighter plasma (from the plasma sheet), with the centrifugal force playing a role analogous to gravity.

[17] Figure 1 follows the formation and growth of one interchange finger (indicated by an asterisk) through the stages of this instability. First, very small scale perturbations (not visible in Figure 1) occur at the interface between the two regions, growing until a spherical bubble of the heavier (cooler temperature in Figure 1) plasma begins to move into the lighter (hotter temperature) plasma (Figure 1a). Injection fingers then grow between the bubbles of heavy plasma, followed by the development of structure on the outward moving fingers themselves due to convection. The tips of the outflowing fingers spiral around so that the tip protrudes out in a mushroom shape. This behavior and shape are similar to the theoretical descriptions detailed by *Sharp* [1984] and *Ramaprabhu and Dimonte* [2005]. The cold heavy plasma finally moves far enough out into the lighter plasma, such that the finger becomes very narrow at the base, or breaks off entirely. At distances shorter than a few Saturn radii, a cooler finger grows straight radially outward, to about 10–12 R_S before Saturn's magnetic field is no longer strong enough to enforce rigid corotation. This effect causes the finger (labeled with an asterisk) to slip and complete slightly less than a full rotation in 10.5 h (i.e., between 18, Figure 1a, and 28 h, Figure 1f). Both numerical and experimental analysis have shown that a Rayleigh-Taylor interchange finger may only grow to 20–100 times its width before it eventually breaks up [*Sharp*, 1984], consistent with the present simulations. At this point the outwelling finger has not yet gained enough energy to break away from the region dominated by corotation (Figure 1i).

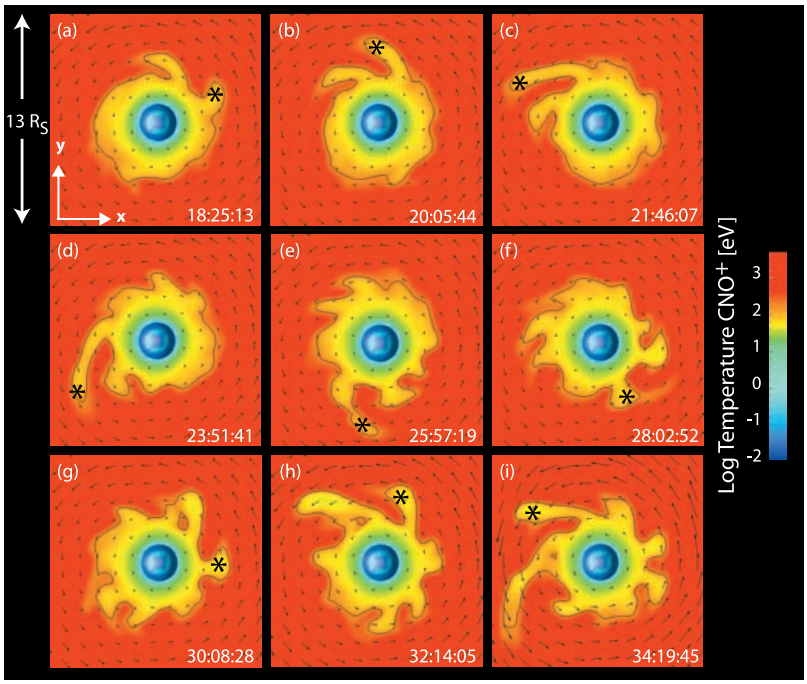

Figure 1. Growth and development of a single outwelling interchange finger (labeled with an asterisk), over slightly less than one and a half rotations of the planet. View of the equatorial plane in the inner magnetosphere. (a and b) Heavier, cooler plasma begins to move into the lighter, hotter plasma. Both these cool, heavy and hot, tenuous structures are referred to as interchange fingers, either as an inward moving or outward moving component. (c and d) Injection fingers grow between the bubbles of heavy plasma. (e–g) The tips of the outflowing fingers protrude out in a mushroom shape. (h and i) The cold heavy plasma moves far enough out, such that the finger becomes narrow at the base.

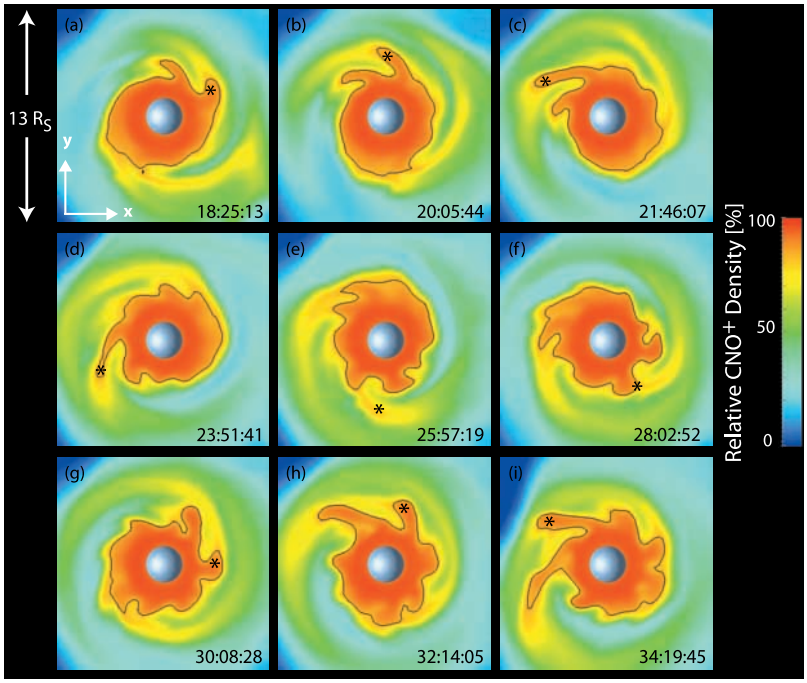

Figure 2. (a–i) Growth and development of a single outwelling interchange finger (marked with an asterisk and over the same time series as in Figures 1a–1i) for relative density of CNO^+, i.e., the % of total ions that are CNO^+. The regions where the CNO^+ population dominates the percentage of total ions aligns well with the cooler temperature fingers.

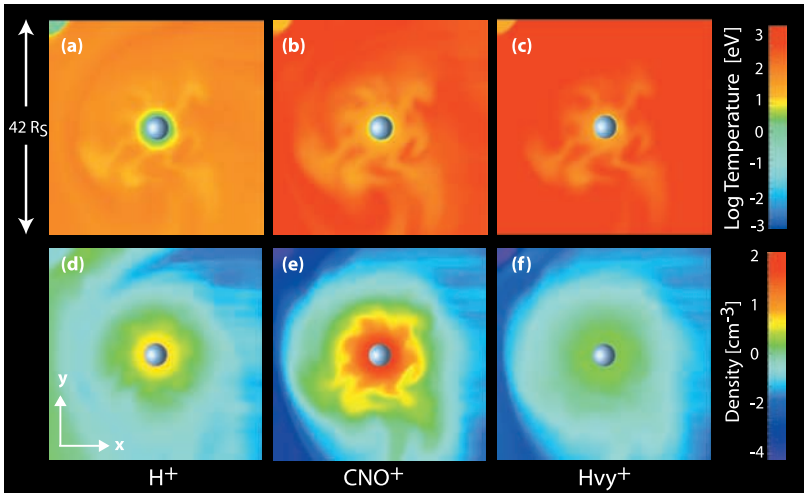

Figure 3. (a–c) Temperature and (d–f) density viewed in the equatorial plane for the three ion species (H^+, CNO^+, and Hvy^+) for a single time, 5219:40 UT.

After enough time has elapsed for the outwelling, cold fingers to fully form (i.e., between 2–3 rotations, or 20–30 h) an individual finger may have enough energy to break away and travel down the tail.

[18] While the Rayleigh-Taylor type instability that develops in Figure 1 moves cool, denser plasma outward, hot injection fingers, interspersed between the cool fingers, are forced radially inward by an $\vec{E} \times \vec{B}$ drift (from the solar wind convection electric field and planetary magnetic field). Much work is currently being undertaken to determine the exact mechanism that cools and then redistributes the hot injected plasma back out as part of the cool outwelling plasma [e.g., *Hill et al.*, 2005; *Rymer et al.*, 2007] after it has been injected as a result of Rayleigh-Taylor and the $\vec{E} \times \vec{B}$ drift. *Rymer et al.* [2008] believe that energy-dependent gradient and curvature drift dispersion moves the injected plasma onto cold inner magnetospheric plasma, at which point it is transported back out with the cold plasma.

[19] The injection regions are both hotter (as shown in Figure 1) and lower density than the outward moving regions. Figure 2 shows the same results as Figure 1 in terms of percentage of CNO^+. The regions where the CNO^+ population dominates the percentage of total ions, aligns well with the cooler temperature fingers. As this RT-type instability develops, cool, dense Enceladus torus plasma interchanges with hotter tenuous plasma. For relatively medium to low densities, interchange is not present, but higher densities ($\sim$10 cm^{-3}) leave the plasma unstable to centrifugal interchange thereby reducing the densities in the inner magnetosphere.

[20] With the injection of hot plasma sheet plasma into the inner magnetosphere we see inward moving channels of plasma that are roughly 0.5 R_S wide (Figure 2i). This is in agreement with the narrow injections seen by *Hill et al.* [2005] of (1/2 R_S) in width. This may be partially explained by the fact that curvature and gradient drift speeds are high at Saturn and as a result the injected ions may quickly drift out of the inward moving flux tube.

[21] Figure 3 shows cuts in the equatorial plane of the temperature and density for a single time. All three ion species are seen without the black contours used to outline the interchange fingers in Figures 1, 2, 4, and 6–8. Cool, dense outward moving fingers are seen in the temperature profiles of all three ions: H^+, CNO^+ and Hvy^+. These fingers are most clearly seen in CNO^+ (Figures 3b and 3e). While the medium mass ions dominate, the Hvy^+ fingers (Figures 3c and 3f) are fainter and more smeared out, probably owing to the larger gyroradius of this heavier ion along with its small initial density.

3.2. Centrifugal Interchange Increases During Antiparallel IMF

[22] The presence of interchange fingers is strongly linked to the direction of the IMF. Figure 4 shows a marked decrease in both the length and number of cool fingers as the IMF flips from an antiparallel (Figure 4a) to parallel orientation (Figure 4i). The time for this change to take effect is only a couple of hours. The tips of the outwelling fingers become thinner, as a result of them shortening and moving back into a region of stronger magnetic field.

[23] It is strikingly evident in our simulation that centrifugal interchange occurred more often during times of antiparallel IMF. During parallel IMF (beginning at Figure 4i), no more than two or three stubby fingers form, but all with lengths no greater than a few Saturn radii. When the IMF turned antiparallel, the overall number of interchange fingers increased (between 7–9) dramatically over 10 h, or one rotation period. This lends confidence to our conclusion that the orientation of the IMF has a noticeable effect on what appears to be a rotationally driven phenomenon taking place in the inner regions of a large magnetosphere.

[24] External conditions are stimulating Saturn's rotationally dominated inner magnetosphere. This may be explained by looking at the plasma sheet. In Figure 5 we see that during parallel IMF the solar wind (which comes in at an angle, as a result of Saturn being tilted relative to the orbital plane) dynamic pressure pushes the plasma sheet up out of the equatorial plane into a "bowl shape". This is consistent with initial Cassini findings that showed the spacecraft rarely crossing the plasma sheet, potentially as a result of its being pushed upward into this bowl shape [*Arridge et al.*,

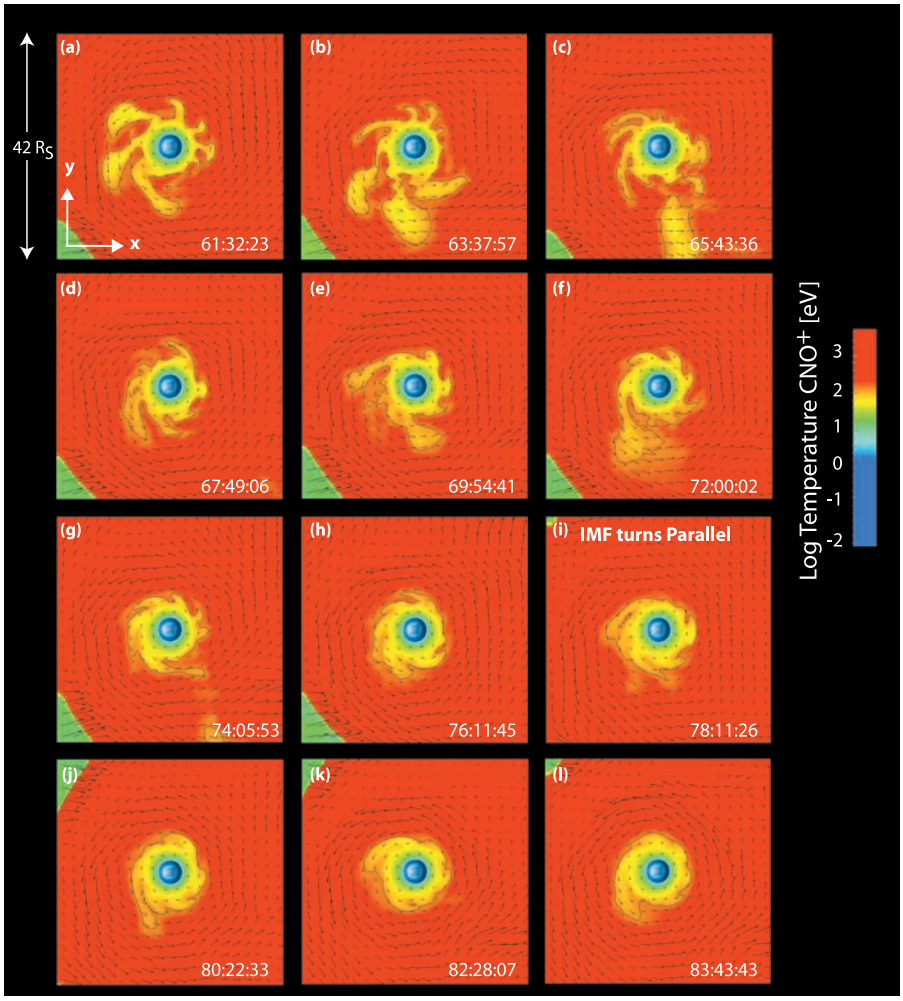

Figure 4. Time series (temperature of CNO^+) showing the effect of switching from antiparallel IMF to parallel IMF on the length and width of the interchange fingers. As the IMF flips from (a–h) an antiparallel to (i–l) a parallel orientation, both the length and total number of interchange fingers decreases.

2007a]. The very large and dynamic dayside current sheet extends to the dayside magnetopause and the current sheet is observed to be highly sensitive to upstream solar wind conditions [*Arridge et al.*, 2007b, 2008]. For parallel IMF (Figure 5, top) we see a thick plasma sheet (~2 R_S half-width on the dayside), in agreement with values adopted by models [*Arridge et al.*, 2007b]. When the IMF turns, the antiparallel IMF now allows the solar wind increased access to the cusps through open field lines (Figure 5, bottom). Reconnection in the higher, bent portion of the "bowl" loads the plasma sheet with additional mass, and centrifugal forcing moves this mass down into the equatorial plane.

[25] As the change in direction of the IMF enables the solar wind to push the mass of magnetodisc down into the equatorial plane, we simultaneously observe a marked increase in the number of interchange fingers forming and their length grows from a few R_S to more than 10 R_S. This occurs over about 15–18 h, or over slightly more than one planetary rotation.

[26] By flattening the plasma sheet as described above, the IMF mass loads the equatorial plane. The fact that an increase in the mass of the equatorial plane contributes to the growth of interchange fingers makes sense in terms of the Rayleigh-Taylor instability. It has been confirmed numerically and experimentally that the development of the RT instability is strongly affected by the Atwood number, a measure of how the densities govern the flow [$A = (\rho_H - \rho_L)/(\rho_H + \rho_L)$], where ρ_H and ρ_L are the densities of the heavier and lighter fluids, respectively [*Youngs*, 1984]. A higher Atwood number will result in outwelling fingers forming faster than the inward bubbles [*Ramaprabhu and Dimonte*, 2005], and greater development of the RT instability. Therefore, it is logical that an increase in the density of the heavy magnetospheric ions at Saturn will lead to an increased Atwood number and in turn larger outward moving fingers.

3.3. Mass Loading the Enceladus Torus Increases Development of Centrifugal Interchange Fingers

[27] Now that we have examined the instability and drifts necessary for centrifugal interchange to occur, let us examine the role of heavy ions more closely. Figure 6 follows centrifugal interchange over one planetary rotation. The IMF is parallel to the planetary field here, so it is initially

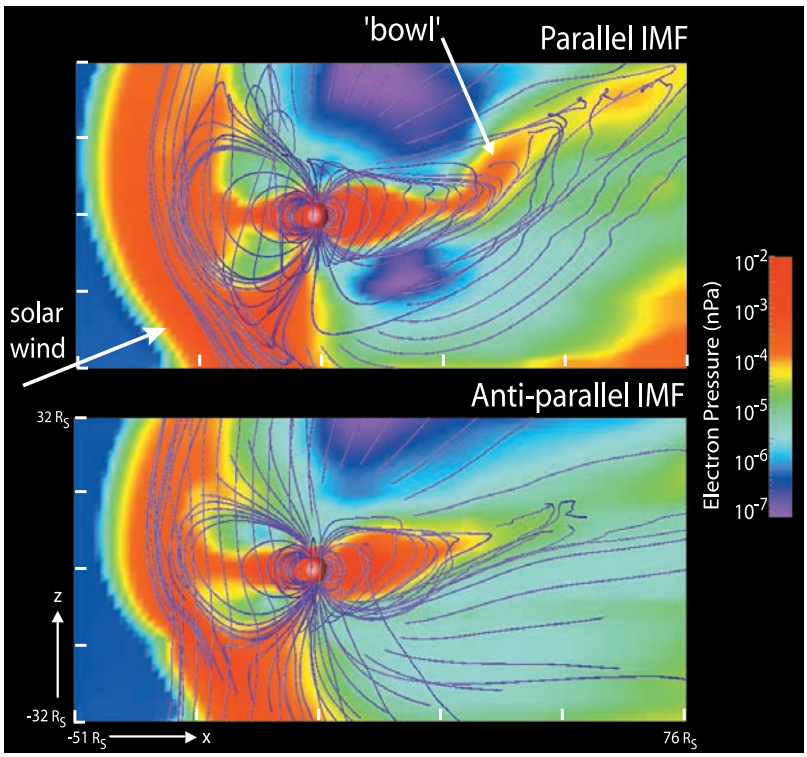

Figure 5. (top) "Bowl"-shaped current sheet during parallel IMF due to the angle of the solar wind, contrasted with (bottom) a flattened current sheet as a result of antiparallel IMF, loading more mass into the equatorial plane. The increased mass subsequently leads to the development of more centrifugal interchange fingers.

expected that as in Figure 4, little to no centrifugal interchange will occur. However, by doubling the concentration of the CNO^+ and Hvy^+ populations, interchange fingers with increased length and width at their tips are seen to occur (relative to the purely antiparallel case with no increase in CNO^+ or Hvy^+ densities). Elevated ion densities in the vicinity of Enceladus may occur during active plume ejection. Note, however, that Figure 6 shows a case in which the CNO^+ and Hvy^+ densities were increased everywhere, not asymmetrically or in a specific section of the torus.

[28] The effect of doubling the concentration of the CNO^+ and the Hvy^+ populations is immediately evident, as seen in Figure 6. The short, stubby interchange fingers normally present during parallel IMF are replaced with a greater number of interchange events (e.g., compare to Figure 4), but the outwelling fingers become wider and spread out azimuthally at a distance of 20 R_S. Again, this makes sense in terms of the increase in the concentration of the heavy ions, leading to an increase in the Atwood number, as discussed above. This is in agreement with *Yang et al.*'s [1994] convective simulations of interchange fingers in the inner Jovian magnetosphere for the case in which one side of the Io torus is loaded with additional mass, leading to fingers forming predominantly on this side.

[29] Injection fingers and outwelling fingers form on time scales that are rapid compared to Saturn's rotation period, but can persist and corotate with the planet for several rotations. In agreement with *Hill et al.* [2005] and *Chen and Hill* [2008], the age of the injection events is clustered under one rotation, but with at least 1–2 fingers surviving >10.5 h, and a few persisting longer than two rotations. The simulation results show that determining the lifetime of an individual finger may be difficult since the fingers evolve as they rotate. There are, on average, 1–2 fewer fingers in this case of increased density, compared to the antiparallel case. Before it reaches the dawnside, a finger may be loaded with sufficient mass so that its length extends beyond the region of the magnetosphere that is dominated by corotation. As the interchange fingers rotate with the planet's period, frequently an individual finger is seen to bend backward (opposite of corotation) at roughly 6 Saturn Local Time (SLT) as a result of being compressed by the magnetosheath (see Figure 6 time series and schematic diagram). As the finger grows out into the magnetosheath and approaches the magnetopause, it finds itself compressed, and all or a portion of it becomes bent backward (Figures 6c–6f). Once Saturn has rotated around to the dayside, the finger is sufficiently stretched such that its tip may break off (Figure 6j) (this does not appear to occur with every rotation, but roughly on the order of every 25 h). A schematic following the rotation of a single interchange finger is shown in Figure 6. These observations are similar to events seen by *Hill et al.* [2005], and may arise from the breaking of the fingers as they propagate down the tail and exceed the magnetic field stress (i.e., essentially becoming super-Alfvénic).

[30] The dynamics occurring at the edges of the outwelling fingers (now fatter as a result of mass loading) are clearly important. By calculating and plotting the Alfvén and sonic Mach numbers (Figures 7b and 7c) we see that the

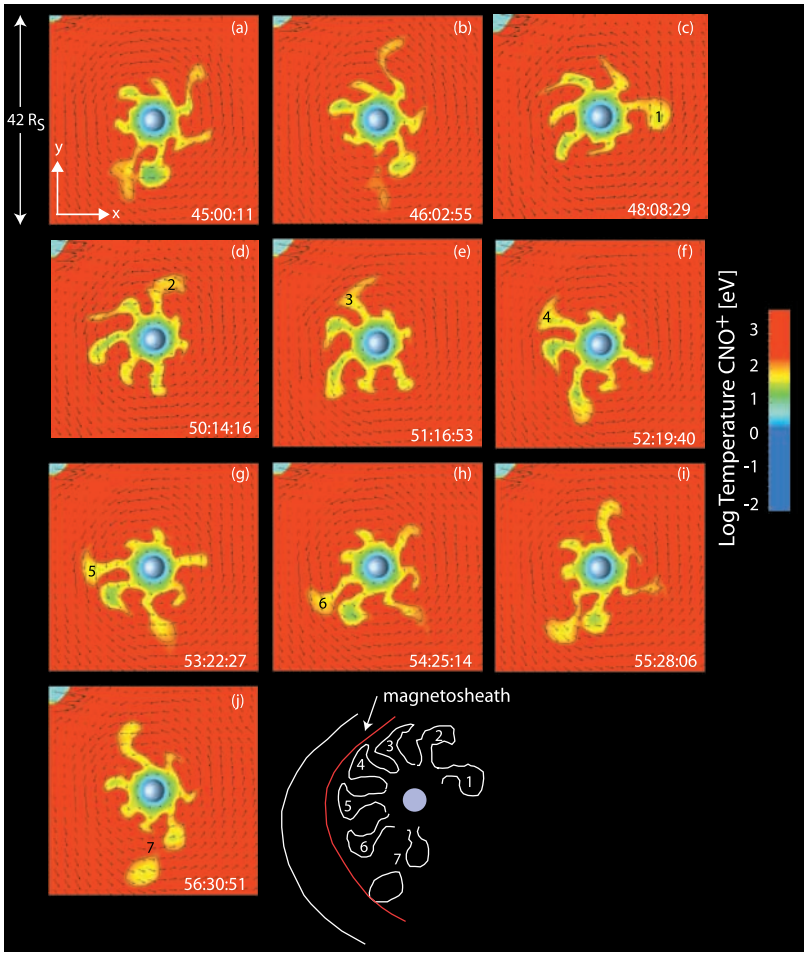

Figure 6. (a–j) Evolution of cooler, outwelling interchange fingers for the case with parallel IMF and double the initial concentration of CNO^+. Parallel IMF is expected to produce few interchange fingers, as noted in Figure 4. However, by elevating the ion densities in the vicinity of Enceladus the mass in the equatorial plane increases, as does the number of interchange fingers present. The single, numbered finger in Figures 6c–6j is first bent backward and compressed by the magnetosheath before being flung out on the duskside. Final schematic drawing follows the growth of this numbered finger.

tips of the outward moving interchange fingers (black contour line) are super-Alfvénic and supersonic. This corresponds to the fact that both the magnetic field and ion density fall off significantly with radial distance. The increased mass being flung toward the tips of the fingers leads to slippage (particularly on the dayside) from rigid corotation (Figure 7a), in agreement with slower spiral motion at the tips of the fingers discussed in section 3.1.

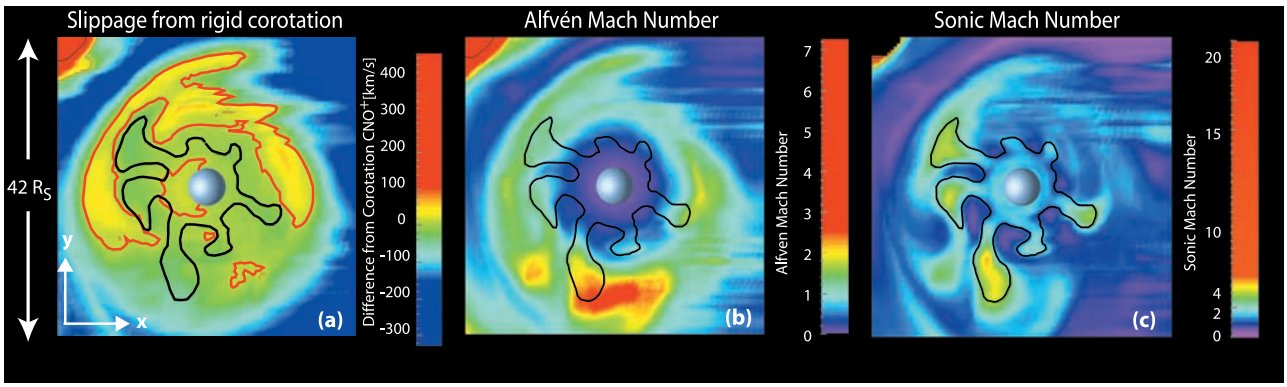

Figure 7. (a) Difference from perfect corotation (red outline = 0 km/s) for CNO^+. Black outline is the temperature contour from Figure 6f. (b) Alfvén Mach number and (c) sonic Mach number.

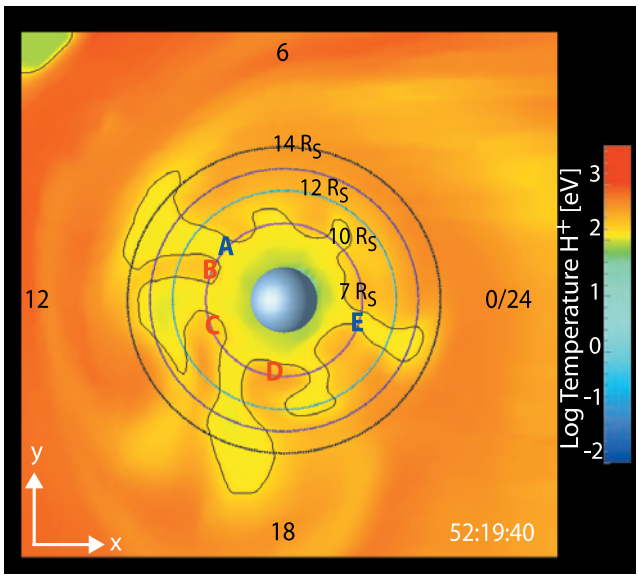

Figure 8. Four model trajectories (magenta, cyan, purple, and black dots) used to generate synthetic spectrograms. All paths begin at midnight SLT and progress counterclockwise through different regions of the interchange fingers.

3.4. Synthetic Spectrograms Consistent With Cassini Bulk Parameters

[31] To confirm that the numerous fingers seen on a global scale in the multifluid model are indeed related to the individual interchange features seen by Cassini at Saturn and consistent with the energies, densities, magnetic fields and temperatures reported by *Burch et al.* [2007], we examine the energy characteristics of the plasma as a function of azimuthal angle at four different radii (7 R_S, 10 R_S, 12 R_S and 14 R_S in Saturn's equatorial plane, trajectories labeled in Figure 8). All of these model trajectories begin at midnight SLT and continue counterclockwise around the planet enabling the model spacecraft to pass through anywhere from two to seven regions of alternating cool and hot plasma, depending on the radial distance of the trajectory, before returning to midnight. The path of this synthetic trajectory was chosen so as to obtain the best path through multiple hot injection fingers and cool outwelling fingers at different SLT and radial distances for comparison with published data. The results in the previous sections indicated that solar wind conditions will strongly affect the formation of interchange fingers thus making more quantitative comparison difficult at best.

[32] By sampling the electron density along these trajectories, density depressions are seen to be associated with the hotter finger-like regions (Figure 9a plots the electron density along the trajectory at 7 R_S). Electron density depressions (labeled B, C and D for the corresponding injection fingers B, C and D in Figure 8) are consistent with comparable decreases in the electron density during injection events observed by the Cassini ELS [*Burch et al.*, 2005], as well as the highly variable electron densities seen outside 5 R_S by *Persoon et al.* [2005]. Examples shown by *Burch et al.* [2005, 2007] show injection events that have these same characteristic signatures. Peak ion temperatures are observed to be on the order of ~1 keV, while the temperatures in the tenuous regions are on the order of ~100 eV. These values are in qualitative agreement with the model results. The abrupt drop in electron density when moving from a cold to a hot flux tube is believed to make the hot, tenuous flux tube sufficiently buoyant to quickly move it in toward the planet [e.g., *Thorne et al.*, 1997].

[33] A specific example [cf. *Burch et al.*, 2005, 2007, Figure 1] shows energy enhancements of a factor of 100, density decreases by a factor of 10, temperature increase by a factor of 10 and magnetic field increases (for injections in the equatorial plane) of 3 nT. These values are consistent with those observed in the simulations. The density decreases by nearly a factor of 10 (Figure 9a). The bulk temperature increases from ~10 eV to ~100 eV (Figure 9b). The magnetic field magnitude increases by 2–3 nT when traversing a finger (Figure 9c). These magnetic field residuals are plotted by estimating the magnetic field component not

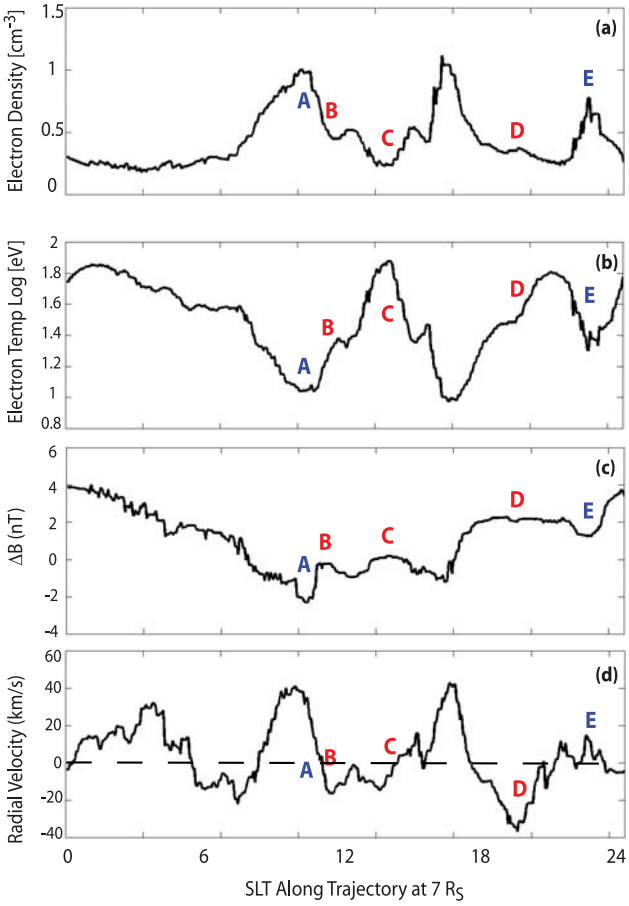

Figure 9. (a) Electron density, (b) electron temperature, (c) magnetic field residuals (above background), and (d) radial velocity (>0 flowing outward, <0 flowing inward) for model trajectory seen in Figure 8 at radial distance of 7 R_S. Density depressions, temperature increases, magnetic field enhancements, and negative radial velocities correspond to the inward moving hotter injection fingers (indicated by B, C, and D). The outwelling plasma has decreased temperature and magnetic field along with increased density and positive radial velocities (indicated by A and E) in agreement with CAPS observations [cf. *Burch et al.*, 2007, Figure 1].

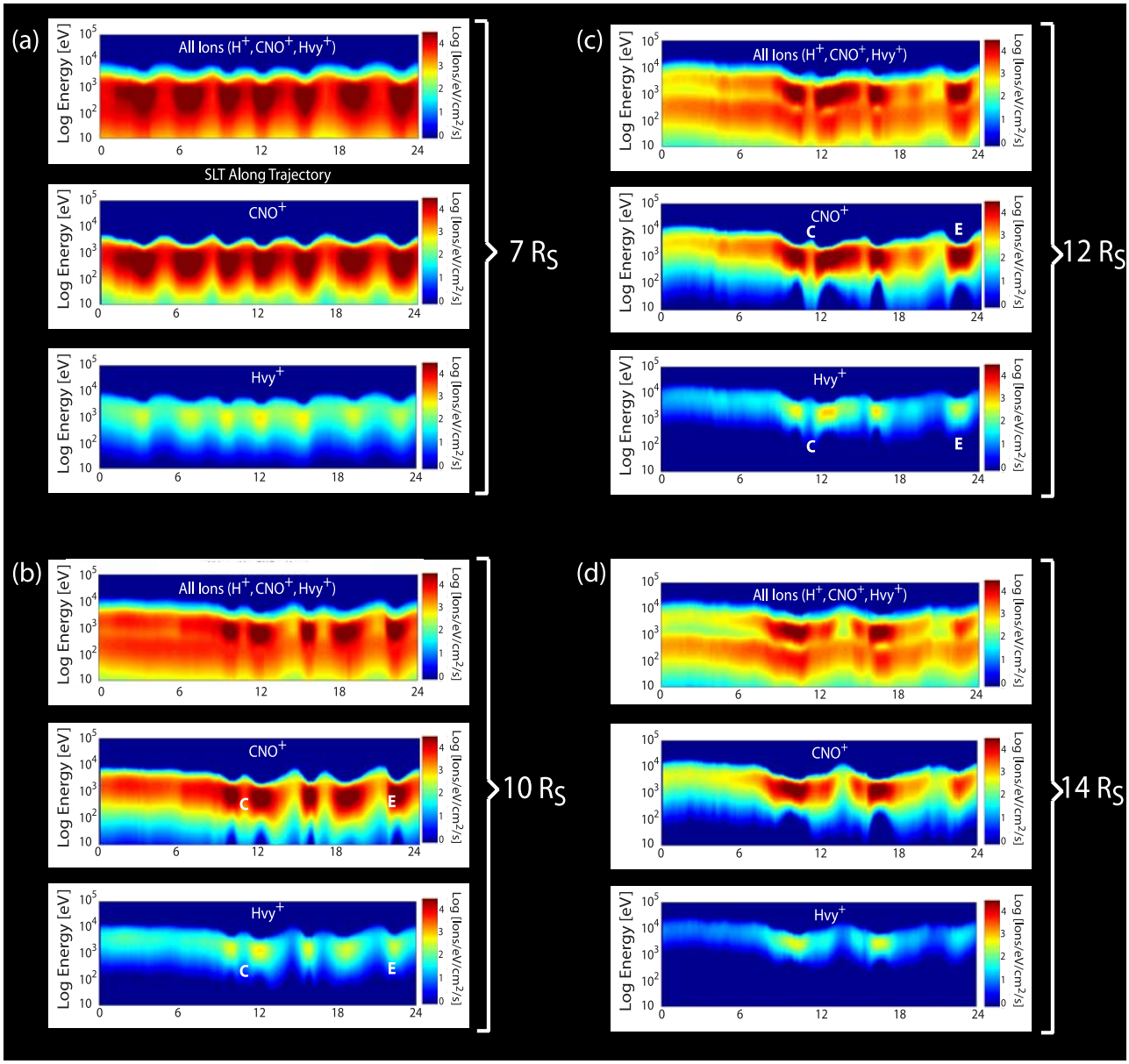

Figure 10. Synthetic spectrograms generated by the multifluid model along the trajectories labeled in Figure 8. The model splits the total ion spectrogram (first panel in each group) into spectrograms of individual ion components (CNO^+ and Hvy^+ are the second and third panels in each group). (a) The innermost trajectory at 7 R_S passes through multiple outward moving, cooler fingers and alternating regions of hotter, inward moving plasma. (b) The 10 R_S trajectory passes through fewer interchange fingers. The portion labeled C indicates an inward moving higher energy injection finger, whereas E (following labels in Figure 8) indicates an outward moving, higher-flux interchange finger. (c) Further out at 12 R_S, the thermal velocity of the Enceladus Hvy^+ increases relative to the ionospheric H^+, giving the total ion spectrogram a double-banded structure. (d) The final 14 R_S trajectory only passes through two outwelling interchange fingers.

from Saturn's dipole. The energy spectrograms (Figure 10, discussed below) also show enhancements similar to the observations.

[34] The multifluid model enables us to generate synthetic spectrograms along any desired trajectory for comparing energy and flux measurements with Cassini data by recording the velocity, temperature and density of each ion population along the path picked out for the model trajectory, and assuming a Maxwellian to determine the probability distribution. Figure 10 plots synthetic spectrograms which include all three of the ion species over an energy range from 10 eV to 100 keV. The model has the added benefit of tidily allowing us to split the total ion spectrogram into spectrograms of individual ion components (H^+, CNO^+ and Hvy^+).

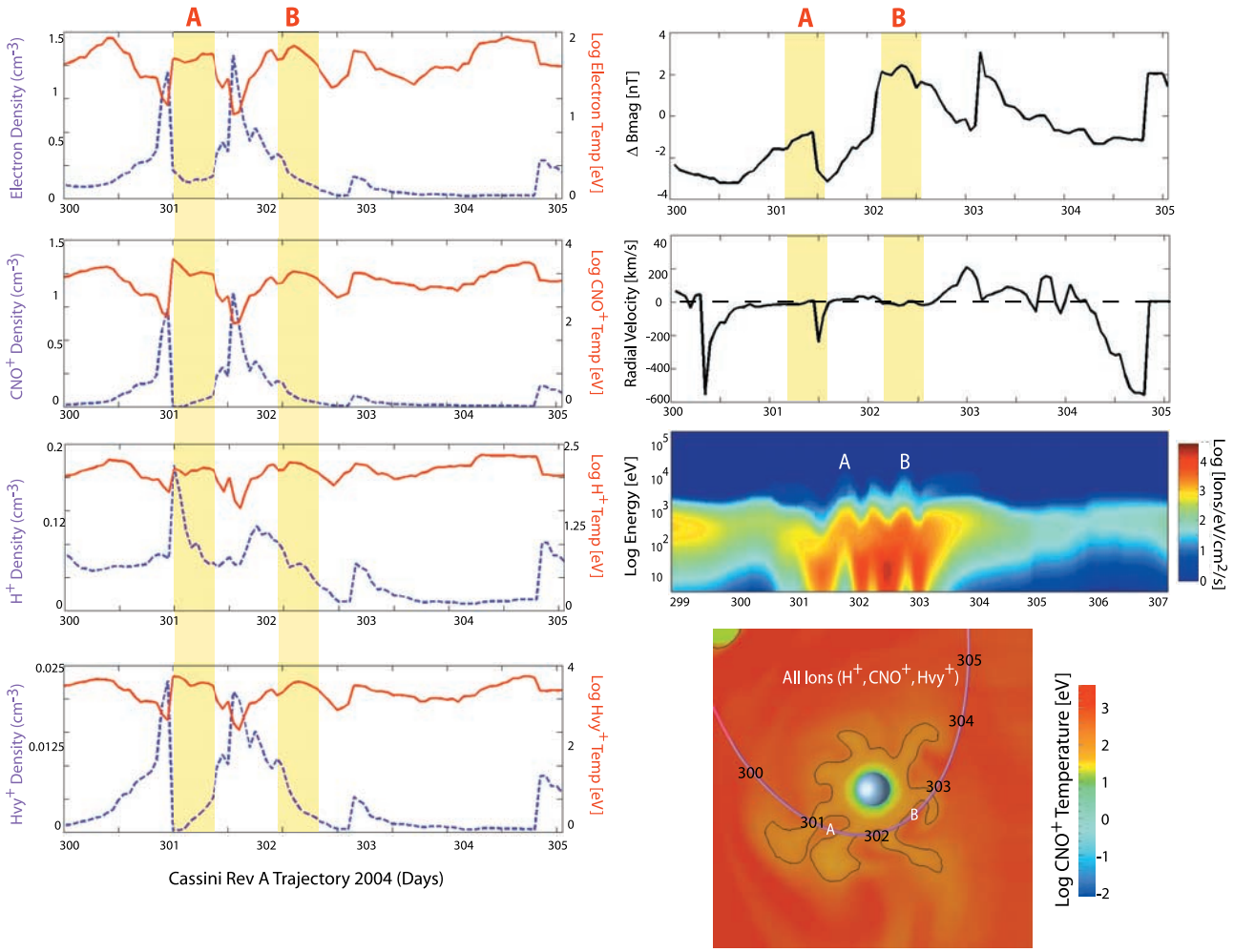

Figure 11. Traces along the Cassini Rev A trajectory for days 300–305, 2004. Plots show temperatures for all species (electrons, H^+, CNO^+, and Hvy^+) and densities for all species (electrons, H^+, CNO^+, and Hvy^+). ΔB is the nondipole component of the magnetic field; also shown are the radial component of the plasma velocity and a synthetic spectrogram of all the ions.

[35] The innermost trajectory (Figure 10a at 7 R_S) passes through seven outward moving cooler fingers and seven regions of hotter inward moving plasma, as is evidenced by the clear increases in CNO^+ flux when passing through the outward moving interchange fingers. Looking at the Hvy^+ spectrogram for the 7 R_S trajectory, the higher-energy ions arrive before the lower-energy ions, a drift dispersion signature. Moving outward to 10 R_S (Figure 10b) this trajectory passes through the middle of three outwelling fingers and the very edge of the last finger. An injection event, labeled C, and outwelling, labeled E, exhibit energies in agreement with *Burch et al.* [2005], which shows energies of 10 keV when Cassini traveled through an injection finger and energies on the order of 1 keV when traversing a cool, dense region. The synthetic electron spectra (not shown) show an order of magnitude change between the inflowing and outflowing channels, while the observed electron spectra show 1–2 orders of magnitude change. The discrepancy between the model peak energies and the observed peak energies is most likely due to the fact that the model does not include high-energy tails produced by wave-particle interactions. *Menietti et al.* [2007] found ubiquitous wave activity in the vicinity of the interchange regions. This will lead to higher peak energies in the observations.

[36] The injection channels in the spectrograms appear much narrower than their outward moving counterparts (Figure 10c). However, looking at the global picture, Figure 6h suggests that this is a sampling effect; the injection region may appear narrower owing to the fact that the cool dense regions expand radially once they move past ~12 R_S as the ambient pressure is less than the pressure of the dense finger. Inside 12 R_S the pressures are such that the outflow and inflow channels have a similar width. Further out at 12 R_S (Figure 10c) the thermal velocity of the Enceladus Hvy^+ ions increases relative to the ionospheric H^+, from 1 to 10 keV as it is picked up, giving the total ion spectrogram a double-banded structure similar to that seen by *Young et al.* [2005], extrapolated to be heavy ions and protons. As the model spacecraft travels through the middle of two and the tip of two other outward fingers, we also see that these fingers are accelerated to a narrower range of energies. Figure 10d (at 14 R_S) shows only two outward fingers, and the narrowness of the injection event B is evident.

[37] The actual radial movement of the plasma is difficult to discern in a single figure, because radial velocities are much smaller than the rotation velocities. This radial motion is also difficult to extract from spacecraft data, partly explaining why the majority of centrifugal interchange events observed have been injections [*Sittler et al.*, 2006; *Rymer et al.*, 2008]. In order to view the radial movement more clearly, the radial component of the velocity is plotted in Figure 9d versus the 7 R_S trajectory in Figure 8, and has two components, those moving radially inward (<0) and outward (>0).

[38] Figure 11 shows plots similar to those in Figure 9, for the Cassini Rev A trajectory from days 300–305, 2004. Cassini entered the dayside magnetopause, traversed the duskside close to the planet before exiting on the dawnside. As the spacecraft passes through inward moving regions of plasma the temperature increases and the density decreases. This is most evident for the electron, CNO^+ and Hvy^+ plots and less so for the H^+ plots. The comparison between the model flybys and spectrograms with Cassini data from *Burch et al.* [2005] are not exact, as no two fingers are alike and the IMF conditions have a marked effect on the nature of the interchange fingers. What is notable is the similarity of the bulk parameters when flying through an injection region (in either the model or Cassini trajectory (Figures 9–11)). When passing through an injection finger, the temperatures increase and the densities decrease.

[39] As in Figure 10, the synthetic spectrogram (Figure 11) shows the higher-energy injections as well as all the ions: the broad H^+ component, the higher-energy Hvy^+ species near the injections and the lower-energy, higher-flux CNO^+ component, also near the injection fingers. The spectrograms taken at different Saturn radii in Figure 10 prove useful in showing changes in the double-banded structure that occurs as fresh ions from the inner magnetosphere are energized. As no two fingers are alike, the details of the plots and spectrograms will be different for various trajectories. One difference between a model flythrough and a spacecraft flyby is that in a model the cuts are at a fixed time, whereas an actual spacecraft experiences the variations in both time and space. Although solar wind conditions are not well constrained for Cassini trajectories, and as this paper endeavors to show, the external IMF conditions have a dramatic effect on the interchange cycle, changes in the bulk parameters (increased temperatures and decreased densities for the inward moving injections) demonstrate that the multifluid treatment has the ability to model the interchange cycle.

[40] To summarize, both the multifluid model (Figures 8–11) and the Cassini spacecraft [*Burch et al.*, 2005, 2007] see the same bulk parameters in the injection fingers: hotter temperatures, decreased ion and electron densities, increased ion and electron energies, increased magnetic field strength in the equatorial plane and radially inward moving plasma. The values of the plasma parameters as determined within these regions are also on the order of those measured by Cassini. We find that these features are ubiquitous and generally centrifugally confined to the equatorial plane, develop during the first ~10 h, before growing to ~20 R_S during a second rotation. Occasionally (>30 h) a blob of cooler plasma is compressed when it rotates into the magnetosheath and is seen to break off from one of the fingers and move downtail.

4. Conclusions

[41] Numerous injection signatures in Saturn's magnetosphere, indicative of a large-scale centrifugal interchange cycle, have been measured by Cassini. This multifluid treatment of the Kronian magnetosphere is the first numerical model to match the bulk parameters (temperature, density, flow direction and energy spectrograms) to observed local injection events. The global nature of the multifluid model allows the spatial structure of both inner magnetosphere processes and global plasma sheet geometry of the interchange events to be characterized.

[42] Future work will focus on the inclusion of a longitudinally asymmetric Enceladus torus, similar to that seen by *Gurnett et al.* [2007], as the current case is for a uniform ion distribution. A localized density enhancement in a portion of the torus, as would more accurately reflect the physics of a plume ejection, similar to that described by *Tokar et al.* [2006] would also be of interest. Additionally, implementation of high-resolution gridding over the inner magnetosphere of the system will improve the ability of the multifluid model to examine ion cyclotron and mass effects in Saturn's large magnetosphere. Boundaries between outward cool, dense plasma with hot, tenuous injections may become sharper as well.

[43] Interchange fingers develop for two configurations: parallel IMF has little to no finger development, while antiparallel IMF has the greatest total number of fingers (1–2 more than the heavy case), but increasing the concentration of heavy ions develops wider outward fingers that may break off entirely. These results indicate that increasing the concentration of heavy ions from Enceladus will render the inner magnetosphere unstable to centrifugal interchange, as will turning of the IMF antiparallel to the planetary magnetic field. Both inner magnetospheric plasma sources (internally driven) and plasma sheet plasma (influenced by the solar wind, externally driven) are determined to play important roles in the development of centrifugal interchange.

[44] While the model does not include a high-energy ring current at this time, the fact that outward diffusion of cold plasma is seen at Saturn [*Sittler et al.*, 2006] suggests that an impoundment effect [*Sergis et al.*, 2007, and references therein] by a hot ring current may not play a large role in modulating the development of interchange events. We see the interchanging plasma move out to a maximum distance of ~20 R_S at which point it breaks up and is not distinguishable from the ambient plasma. Interchange events that have characteristics similar to those observed by Cassini are readily seen in the model, and the model results suggest that the interchange events are strongly controlled by the IMF orientation and mass loading from Enceladus. Any impoundment effect impeding radial transport may be stronger at Jupiter (and possibly why centrifugal interchange events are less frequently observed) as a result of the hotter ring current but the Jovian system is also less sensitive to IMF orientation. Further simulations comparing the Kronian system with the Jovian system are needed resolve this issue.

[45] **Acknowledgments.** This work was funded by NASA grants NNX07AJ80G and NNX08AR16G.

[46] Wolfgang Baumjohann thanks the reviewers for their assistance in evaluating this paper.

References

André, N., M. K. Dougherty, C. T. Russell, J. S. Lesiner, and K. K. Khurana (2005), Dynamics of the Saturnian inner magnetosphere: First inferences from the Cassini magnetometers about small-scale plasma transport in the magnetosphere, *Geophys. Res. Lett.*, *32*, L14S06, doi:10.1029/2005GL022643.

André, N., et al. (2007), Magnetic signatures of plasma-depleted flux tubes in the Saturnian inner magnetosphere, *Geophys. Res. Lett.*, *34*, L14108, doi:10.1029/2007GL030374.

Arridge, C. S., K. K. Khurana, C. T. Russell, E. C. Sittler, N. André, H. J. McAndrews, A. J. Coates, and M. K. Dougherty (2007a), Periodic crossings of Saturn's magnetospheric current/plasma sheet observed by Cassini CAPS/ELS and MAG, *Eos Trans. AGU*, *88*(52), Fall Meet. Suppl., Abstract P31A-0194.

Arridge, C. S., C. T. Russell, K. K. Khurana, N. Achilleos, N. André, A. M. Rymer, M. K. Dougherty, and A. J. Coates (2007b), Mass of Saturn's magnetodisc: Cassini observations, *Geophys. Res. Lett.*, *34*, L09108, doi:10.1029/2006GL028921.

Arridge, C. S., C. T. Russell, K. K. Khurana, N. Achilleos, S. W. H. Cowley, M. K. Dougherty, D. J. Southwood, and E. J. Bunce (2008), Saturn's magnetodisc current sheet, *J. Geophys. Res.*, *113*, A04214, doi:10.1029/2007JA012540.

Burch, J. L., J. Goldstein, T. W. Hill, D. T. Young, F. J. Crary, A. J. Coates, N. André, W. S. Kurth, and E. C. Sittler Jr. (2005), Properties of local plasma injections in Saturn's magnetosphere, *Geophys. Res. Lett.*, *32*, L14S02, doi:10.1029/2005GL022611.

Burch, J. L., J. Goldstein, W. S. Lewis, D. T. Young, A. J. Coates, M. Dougherty, and N. André (2007), Tethys and Dione as sources of outward flowing plasma in Saturn's magnetosphere, *Nature*, *447*, 833–835, doi:10.1038/nature05906.

Butcher, J. C. (1987), *The Numerical Analysis of Ordinary Differential Equations: Runge-Kutta and General Linear Methods*, Wiley-Interscience, New York.

Chen, Y., and T. W. Hill (2008), Statistical analysis of injection/dispersion events in Saturn's inner magnetosphere, *J. Geophys. Res.*, *113*, A07215, doi:10.1029/2008JA013166.

Fukazawa, K., S. Ogi, T. Ogino, and R. J. Walker (2007), Magnetospheric convection at Saturn as a function of IMF Bz, *Geophys. Res. Lett.*, *34*, L01105, doi:10.1029/2006GL028373.

Gurnett, D. A., et al. (2007), The variable rotation period of the inner region of Saturn's plasma disk, *Science*, *316*, 443–445.

Hansen, K. C., T. I. Gombosi, D. L. DeZeeuw, C. P. T. Groth, and K. G. Powell (2000), A 3D global MHD simulation of Saturn's magnetosphere, *Adv. Space Res.*, *26*, 1681–1690.

Hansen, K. C., A. J. Ridley, G. B. Hospodarsky, N. Achilleos, M. K. Dougherty, T. I. Gombosi, and G. Tóth (2005), Global MHD simulations of Saturn's magnetosphere at the time of Cassini approach, *Geophys. Res. Lett.*, *32*, L20S06, doi:10.1029/2005GL022835.

Hill, T. W., A. M. Rymer, J. L. Burch, F. J. Crary, D. T. Young, M. F. Thomsen, D. Delapp, N. André, A. J. Coates, and G. R. Lewis (2005), Evidence for rotationally driven plasma transport in Saturn's magnetosphere, *Geophys. Res. Lett.*, *32*, L14S10, doi:10.1029/2005GL022620.

Kivelson, M. G., K. K. Khurana, C. T. Russell, and R. J. Walker (1997), Intermittent short-duration magnetic field anomalies in the Io torus: Evidence for plasma interchange?, *Geophys. Res. Lett.*, *24*, 2127–2130.

Krupp, N., et al. (2004), Dynamics of the Jovian magnetosphere, in *Jupiter*, edited by F. Bagenal, pp. 617–638, Cambridge Univ. Press, Cambridge, U.K.

Mauk, B. H., D. J. Williams, and R. W. McEntire (1997), Energy-time dispersed charged particle signatures of dynamic injections in Jupiter's inner magnetosphere, *Geophys. Res. Lett.*, *24*, 2949–2952.

Mauk, B. H., et al. (2005), Energetic particle injections in Saturn's magnetosphere, *Geophys. Res. Lett.*, *32*, L14S05, doi:10.1029/2005GL022485.

Menietti, J. D., P. H. Yoon, and D. A. Gurnett (2007), Possible eigenmode trapping in density enhancements in Saturn's inner magnetosphere, *Geophys. Res. Lett.*, *34*, L04103, doi:10.1029/2006GL028647.

Paty, C., and R. M. Winglee (2006), The role of ion cyclotron motion at Ganymede: Magnetic field morphology and magnetospheric dynamics, *Geophys. Res. Lett.*, *33*, L10106, doi:10.1029/2005GL025273.

Paty, C., et al. (2007), Understanding Enceladus' plume through simulation: Incorporating ion-neutral interactions into 3D multi-fluid modeling, paper presented at Magnetospheres of the Outer Planets Conference, Southwest Res. Inst., San Antonio, Tex.

Persoon, A. M., D. A. Gurnett, W. S. Kurth, G. B. Hospodarsky, J. B. Groene, P. Canu, and M. K. Dougherty (2005), Equatorial electron density measurements in Saturn's inner magnetosphere, *Geophys. Res. Lett.*, *32*, L23105, doi:10.1029/2005GL024294.

Ramaprabhu, P., and G. Dimonte (2005), Single-mode dynamics of the Rayleigh-Taylor instability at any density ratio, *Phys. Rev. E*, *71*, 036314.

Rymer, A. M., et al. (2007), Electron sources in Saturn's magnetosphere, *J. Geophys. Res.*, *112*, A02201, doi:10.1029/2006JA012017.

Rymer, A. M., B. H. Mauk, T. W. Hill, C. Paranicas, D. G. Mitchell, A. J. Coates, and D. T. Young (2008), Electron circulation in Saturn's magnetosphere, *J. Geophys. Res.*, *113*, A01201, doi:10.1029/2007JA012589.

Sergis, N., S. M. Krimigis, D. G. Mitchell, D. C. Hamilton, N. Krupp, B. M. Mauk, E. C. Roelof, and M. Dougherty (2007), Ring current at Saturn: Energetic particle pressure in Saturn's equatorial magnetosphere measured with Cassini/MIMI, *Geophys. Res. Lett.*, *34*, L09102, doi:10.1029/2006GL029223.

Sharp, D. H. (1984), An overview of Rayleigh-Taylor instability, *Physica D*, *12*, 3–18.

Sittler, E. C., Jr., et al. (2006), Cassini observations of Saturn's inner plasmasphere: Saturn orbit insertion results, *Planet. Space Sci.*, *54*(12), 1197–1210, doi:10.1016/j.pss.2006.05.038.

Snowden, D., R. Winglee, C. Bertucci, and M. Dougherty (2007), Three-dimensional multifluid simulation of the plasma interaction at Titan, *J. Geophys. Res.*, *112*, A12221, doi:10.1029/2007JA012393.

Thorne, R. M., T. P. Armstrong, S. Stone, D. J. Williams, R. W. McEntire, S. J. Bolton, D. A. Gurnett, and M. G. Kivelson (1997), Galileo evidence for rapid interchange transport in the Io torus, *Geophys. Res. Lett.*, *24*, 2131–2134.

Tokar, R. L., et al. (2006), The interaction of the atmosphere of Enceladus with Saturn's plasma, *Science*, *311*, 1409–1412, doi:10.1126/science.1121061.

Winglee, R. M. (2004), Ion cyclotron and heavy ion effects on reconnection in a global magnetotail, *J. Geophys. Res.*, *109*, A09206, doi:10.1029/2004JA010385.

Yang, Y. S., R. A. Wolf, R. W. Spiro, T. W. Hill, and A. J. Dessler (1994), Numerical simulation of torus-driven plasma transport in the Jovian magnetosphere, *J. Geophys. Res.*, *99*, 8755–8770.

Young, D. T., et al. (2005), Composition and dynamics of plasma in Saturn's magnetosphere, *Science*, *307*, 1262–1266, doi:10.1126/science.1106151.

Youngs, D. L. (1984), Numerical simulation of turbulent mixing by Rayleigh-Taylor instability, *Physica D*, *12*, 32–44.

A. Kidder, E. M. Harnett, and R. M. Winglee, Department of Earth and Space Sciences, University of Washington, Box 351310, Seattle, WA 98195, USA. (ariah@ess.washington.edu)